

Corrosion investigations of materials in antimony-tin and antimony-bismuth alloys for liquid metal batteries

Tianru Zhang, Annette Heinzl, Adrian Jianu, Alfons Weisenburger, Georg Müller

1. Abstract

Liquid metal batteries are discussed as stationary electrical energy storage for renewable energies, in order to compensate their fluctuating supply of energy.

A liquid metal battery consists of three different liquid, which stay segregated due to density differences and mutual immiscibility. The negative electrode is the low density liquid metal, in our case sodium, a medium density molten salt is the electrolyte and positive electrode is a high density liquid metal. For the latter Sb-Sn and Sn-Bi alloys are selected.

However, one issue is the compatibility of the structural materials with the used liquids. In a first step the behaviour of potential structural materials in Sb_3Sn_7 and SbBi_9 at the temperature of 450 °C up to 750h were tested. The result showed that the corrosion in SbBi_9 was significantly less than in Sb_3Sn_7 and the most promising materials were molybdenum and Max-phase coatings.

Key words: Corrosion, Sb-Sn alloy, Sb-Bi alloy, Liquid metal batteries

2. Introduction

Liquid metal batteries (LMBs) are an intriguing energy storage technology because of its advantages including low-cost, simply assembly, high kinetics on liquid-liquid boundaries, potential for large-capacity and long-lifespan, etc. [1, 2]. Nowadays it has attracted great interest to be applied as one of most promising large scale electricity storage device to smooth over the intermittency of renewable energy production such as wind and solar, in order to integrate them into grid [3-6].

Despite the excellent electrochemical performance of Li-based LMBs, lithium is not an abundant element, there are considerable concerns about the rare natural resources of lithium in the Earth's crust (only 0.0017wt %), uneven global distribution (predominantly in Chile, Bolivia and China) of lithium and expected increasing cost of lithium-ion-containing minerals (Li_2CO_3) [7, 8], which make low cost Na-based LMBs more competitive in large scale energy storage for the future energy system. Therefore, the aim of our research is to realize low-cost Na-based LMBs with good electrochemical performance and long lifetime.

Based on recent researches, Sb is the most promising positive electrode candidate because of its low cost and relatively higher cell voltage, but its high melting point (631 °C) requires undesirable higher cell operating temperature and herein results in higher corrosion rates. Some researchers found that alloying Sb with Pb can significantly decrease the melting point of positive electrode as well as the cell operating temperature without a decrease in cell voltage [3][6]. However, considering about the potential environmental concerns might be brought by large-scale application of Pb, Sn and Bi were selected to alloy with Sn an environmentally friendly positive electrode material with promising thermodynamic and electrochemical performance [6].

The higher operating temperature (usually above 300 °C) of LMBs brings one of the biggest scientific issues to be solved: the compatibility of structural materials with those effective compositions/ corrosion behaviour of structural materials with heavy liquid metal, molten salt and liquid sodium as well.

Up to now, 10 kinds of materials: T91 steel, 304 steel, 316L steel, 4J33 alloy, High-entropy-alloy (HEA), elemental Mo, elemental Cr, 3 Max-phase coatings on Al_2O_3 substrate (Ti_2AlC , Ti_3AlC_2 and Cr_2AlC) were chosen to evaluate their corrosion resistance against heavy liquid metal Sb_3Sn_7 and SbBi_9 , respectively [6], at 450 °C with the duration of 1 month, in order to investigate their potential to be applied as Positive Current Collector (PCC) material in LMBs.

3. Experimental section

Except for those 3 kinds of Max-phases, all test materials were ground before exposure. All specimens were fixed on an Al_2O_3 -holder by Mo-wires and then exposed to liquid Sb_3Sn_7 and SbBi_9 , respectively.

The used facility for this corrosion test is the COSTA facility in the IHM/KIT (Institute of High power and Microwave Technology/Karlsruhe Institute of Technology) lab [9]. It consists of a furnace, which is applied to regulate the isothermal condition for the exposure, and two separately quartz tubes, which are set inside the furnace. The quartz tubes are connected with a gas control system and flow meters to adjust the gas flow and to control the atmosphere.

At the first step, an appropriate temperature gradient was regulated in the three-zone furnace of COSTA facility to achieve the largest possible uniform temperature distribution inside the quartz tubes at the temperature of 450 °C.

The used composition of heavy metal were gained by mixing the individual heavy metals Sb, Sn and Bi in their solid forms together (90 g for both Sb_3Sn_7 and SbBi_9) in Al_2O_3 -crucibles. For this, granular of the metals were used. In the case of Sn the granular had a size of 2-4 mm and a purity of 99.99 %. It was delivered by the company HMW Hauner GmbH & Co. KG; Sb and Bi was delivered by Haines & Maassen. The Sb granular had a purity of 99.65 % and a size of 1-10 mm and the Bi granular had a purity of 99.99 % and a size of 1-3 mm. Unfortunately, the surface of the Bi granular was a bit oxidized, so it had been first melted in a Mo-crucible and the slag layer on top was removed. After that the desired amount of molten Bi was poured into the Al_2O_3 -crucibles and cooled down in room temperature.

After the crucibles were filled, they were put into the furnace at room temperature. Additional, the atmosphere inside the quartz tubes were pre-purged with 100 ml/min $\text{Ar}5\%\text{H}_2$ for 2 days. Then the temperature was raised up to 700 °C to melt as well the Sb (melting point: 631 °C) which has the highest melting point of the 3 metals. The high temperature was hold for 2 hours, afterwards the temperature was decreased to the test temperature of 450 °C. To get a reducing environment inside the liquid metal, it was hold under 100 ml/min $\text{Ar}5\%\text{H}_2$ gas flow.

For loading and unloading of the specimens, a glove box was connected to the quartz tubes. To maintain the atmosphere inside the furnace, the globe box was also purged before with $\text{Ar}5\%\text{H}_2$ gas until an oxygen content of $2 \cdot 10^{-14}$ ppm was reached. For the exposure each specimen were put into the glove box, separately added and full-immersed/sub-immersed (depends on the shape and size of specimens) in one Al_2O_3 -crucible through the globe box with inert atmosphere. Then all Al_2O_3 -crucibles were set back into COSTA facility and held isothermally at 450 °C for exposure duration of 750h.

After 750h exposure in Sb_3Sn_7 and SbBi_9 , all specimens were extracted from the COSTA facility, cooled down in glove box to room temperature and analyzed by XRD, LOM and SEM with EDX.

4. Results and Discussion

The appearance of all samples after exposure to liquid Sb_3Sn_7 and SbBi_9 , respectively, are shown in Fig. 1 a) and b). As shown in this graph, regardless of the two different compositions of the liquid metal systems, the immersed part of all metallic samples were more or less covered by a layer of liquid metal. In contrast, all 3 kinds of Max-phases showed no attachment of liquid metal and all retained their original appearance.

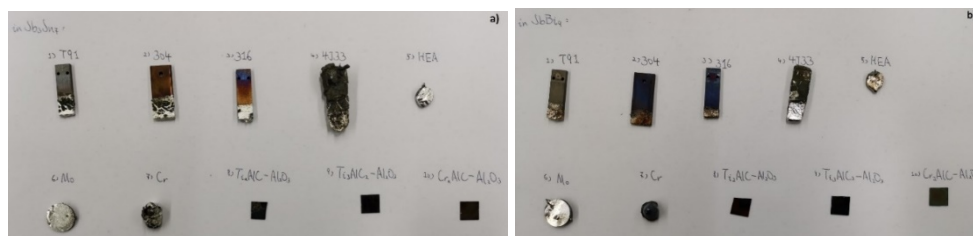


Figure 1: The appearance of all samples after exposure in the circumstance of a) Sb_3Sn_7 and b) SbBi_9

The SEM images of all samples after exposure are shown in following paragraphs. After the exposure, all metallic tested specimens (Mo, Cr, steels and alloys) were cut, embedded into resin, ground and then polished for the observation and examination of cross-sections with the help of SEM. Due to the fact, that nearly no heavy metals was sticking on the 3 kinds of Max-phases, an investigation of the surface of these materials after exposure was possible and done, an investigation of the cross-section was not done so far.

The observation and examination of cross-sections of specimens reveal the microstructure of the interface between the specimen surface and the layer attached and/or formed on the specimen surface during the exposure, which indicates the penetration of heavy liquid metals and the dissolution/destruction of specimen during the exposure likewise.

The elemental mapping/point scanning/line scanning on cross-sections or on surface morphologies determines the distribution of diverse elements including liquid metals at certain spots in specimens.

4.1 304 steel

304 steel was taken as an example, other metallic samples (all the other steels, 4J33 alloy, HEA and Cr), showed similar corrosive performance like 304 steel in Sb_3Sn_7 and in $SbBi_9$ environment, expect for Mo, which has an outstanding corrosion-resistance in both environments.

4.1.1 in Sb_3Sn_7 environment

Fig. 2 shows the cross-sections of 304 steel specimen and its EDX elemental mapping analysis after exposure in Sb_3Sn_7 . A layer of heavy liquid metal (bright part in the first image) was attached on the steel surface and showed on one side a partly enormous penetration into 304 steel. After 750h exposure in Sb_3Sn_7 , the maximal penetration depth in 304 steel is larger than 1 mm. EDX elemental maps reveals that Fe, Cr and Ni were intensively dissolved after exposure in Sb_3Sn_7 . Furthermore, both Sb and Sn in Sb_3Sn_7 showed evident penetration into 304 steel.

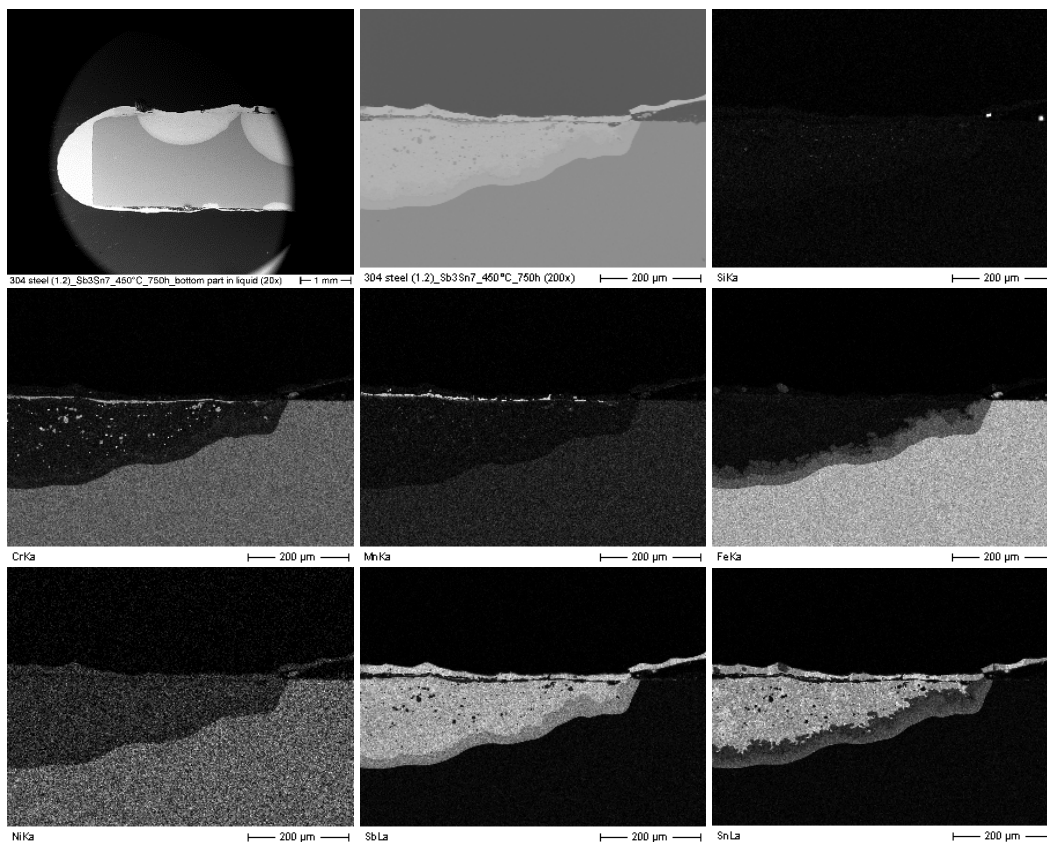


Figure 2: Cross-sections and Elemental maps of 304 steel after exposure in Sb_3Sn_7

4.1.2 in SbBi₉ environment

As shown in Fig. 3, the surface of 304 steel specimen immersed in SbBi₉ was attached by a layer of heavy liquid metal (bright part in the first image) as well. Furthermore, these images also indicate that 304 steel specimen suffered distinct dissolution attack during exposure in SbBi₉; however, compared with Sb₃Sn₇, SbBi₉ exhibited much slighter penetration into 304 steel, the maximal penetration depth after 750h exposure is around 20μm.

EDX elemental mapping analysis across the specimen surface indicates that compared with the specimen in Sb₃Sn₇, dissolution and destruction of 304 steel occurred during the exposure in SbBi₉ is more drastic; however, compared with the Sb₃Sn₇, both Sb and Bi in SbBi₉ did not show severe penetration into 304 steel; furthermore, in comparison to Sb, Bi showed less penetration depth into 304 steel.

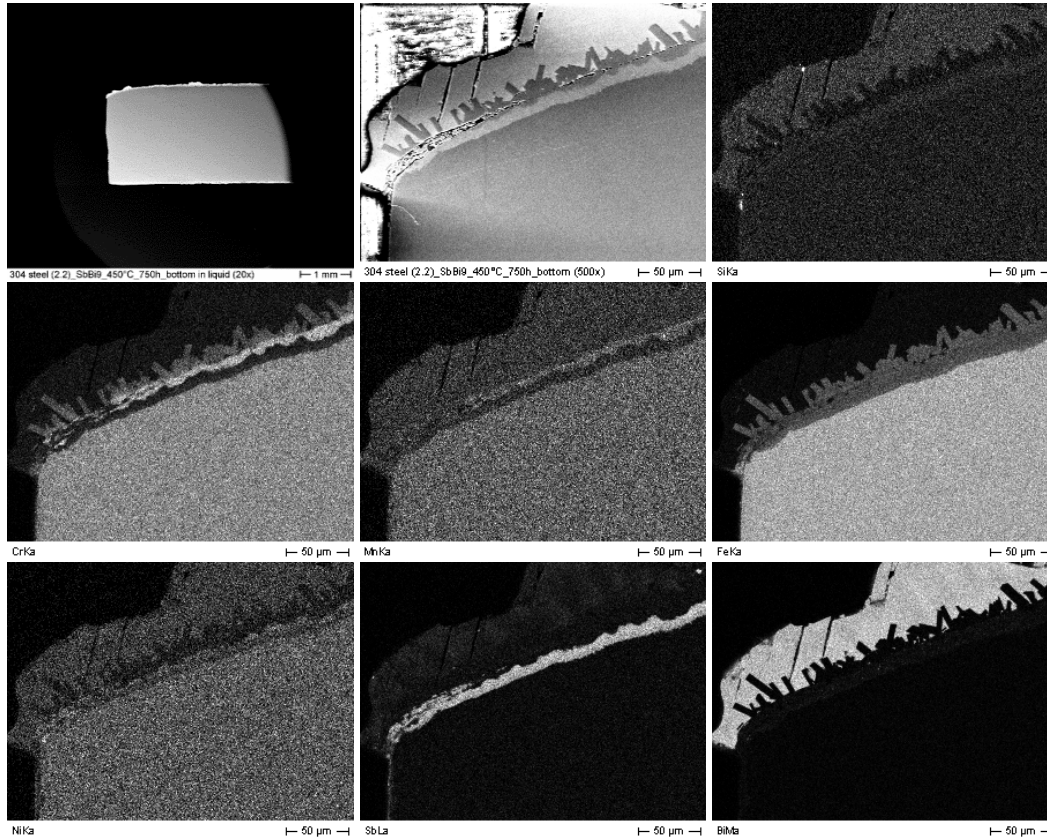


Figure 3: Cross-sections and Elemental maps of 304 steel after exposure in SbBi₉

4.2 Elemental Mo

4.2.1 in Sb₃Sn₇ environment

Fig. 4 shows the cross-sections of Mo specimen and its EDX elemental mapping analysis after exposure in Sb₃Sn₇. Obviously, a layer of heavy liquid metal was attached on the surface of elemental Mo; however, no penetration of Sb₃Sn₇ or development of second phases can be observed into elemental Mo. In addition, EDX elemental maps clarify that elemental Mo suffered no dissolution attack during the exposure in Sb₃Sn₇ for 750h. Furthermore, those images also indicate that both Sb and Sn in Sb₃Sn₇ showed no penetration into elemental Mo.

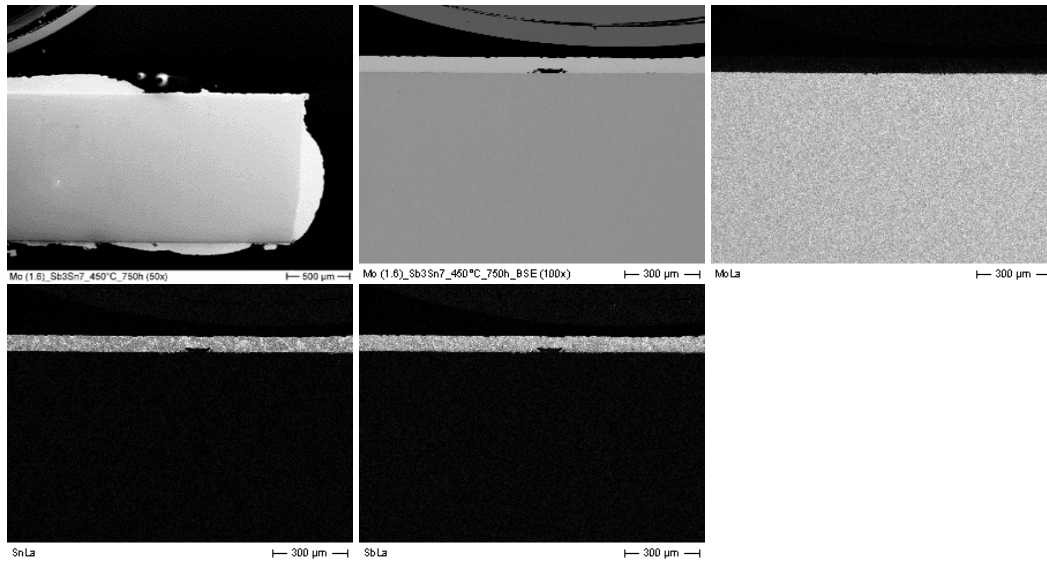


Figure 4: Cross-sections and Elemental maps of Mo after exposure in Sb3Sn7

4.2.2 in SbBi₉ environment

Fig. 5 presents the cross-sections and the elemental mapping analysis of Mo after exposure in SbBi₉, the surface of Mo specimen immersed in SbBi₉ was attached by an extremely thin layer of heavy liquid metal. Similarly, no penetration of SbBi₉ can be observed into elemental Mo in this case. In addition, these images also indicate that elemental Mo specimen suffered no dissolution attack and developed no second phases during the 750 h exposure in SbBi₉ as well. Furthermore, both Sb and Bi in SbBi₉ showed no penetration into elemental Mo.

Fig. 6 shows the line scan across the surface layer of elemental Mo after exposed in SbBi₉ for 750h, which also reveals that both Sb and Bi in SbBi₉ showed no penetration into elemental Mo. The Mo specimen surface were still in good condition after exposure. Therefore, the Mo attached on sample surface might come from Mo powder generated when the sample was cut.

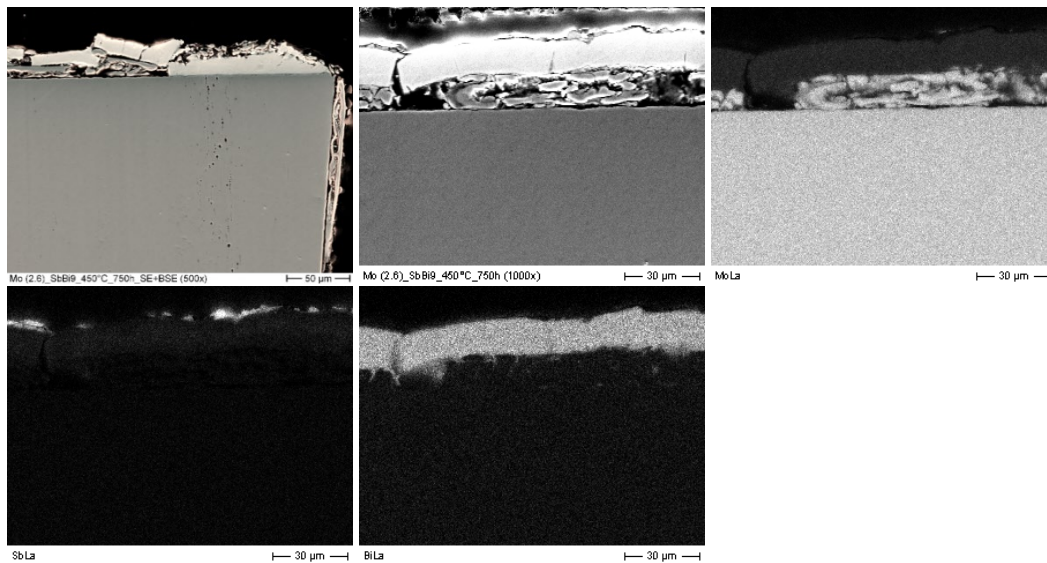


Figure 5: Cross-sections and Elemental maps of Mo after exposure in Sb3Sn7

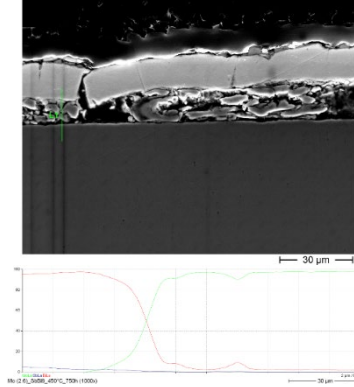


Figure 6: Line scan across the surface layer of Mo after exposure in SbBi9

4.3 Cr₂AlC-Al₂O₃ (Max-phase on Al₂O₃ substrate)

Cr₂AlC coated on Al₂O₃ substrate was also cited as an example, since the other 2 Max-phases showed great similarities on corrosion performance to Cr₂AlC-Al₂O₃ after exposure in those two heavy liquid metal environments.

4.3.1 in Sb₃Sn₇ environment

Fig. 7 presents the surface morphology of Cr₂AlC coated on Al₂O₃ substrate after exposure in Sb₃Sn₇. It can be seen from this figure that the surface of Cr₂AlC-Al₂O₃ specimen kept perfect and smooth; no dissolution attack or penetration of liquid metal were observed after exposure in Sb₃Sn₇. Obviously, some small, bright particles were attached on specimen surface, which were evidenced by EDX elemental mapping analysis, are drops of Sb and Sn.

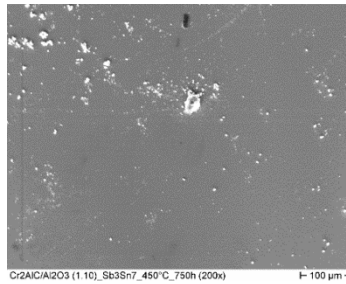


Figure 7: Surface morphology of Cr₂AlC-Al₂O₃ after exposure in Sb₃Sn₇

4.3.2 in SbBi₉ environment

As shown in Fig. 8, the surface morphology of Cr₂AlC coated on Al₂O₃ substrate immersed in SbBi₉ also remained perfect and smooth. No dissolution attack or penetration of liquid metal were observed on Cr₂AlC-Al₂O₃ specimen after exposure in SbBi₉. However, compared with Sb₃Sn₇, the amount of small and bright particles attached on specimen surface in the circumstance of SbBi₉ was much less. Those drops were confirmed by qualitative EDX analysis, as remained Sb and Bi drops.

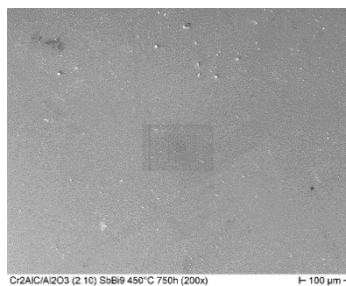


Figure 8: Surface morphology of Cr₂AlC-Al₂O₃ after exposure in SbBi₉

5. Conclusion

It can be seen from the results of all specimens after 750h exposure in these two different heavy liquid metal systems (Sb_3Sn_7 and SbBi_9) at 450 °C that each composition of heavy liquid metal system has its own corrosion property. In comparison to the Sb-Bi system, the Sb-Sn system is highly aggressive and corrosive, which also indicate that it is necessary for us to compare their electrochemical performance when applied as positive electrode in future experiments.

Among all the test materials, all specimens of steels and alloys (T91 steel, 304 steel, 316L steel, HEA, 4J33 alloy) as well as Cr could not meet the corrosion resistance requirements in such heavy liquid metal environments. One except is Mo, the only tested metallic material which shows outstanding corrosion-resistant performance during the exposure; however, for the application of Mo, its higher price (\$ 26000/ton) has to be taken into consideration, which makes the coating of Mo on steel substrate the appropriate method.

All 3 Max-phases (Ti_2AlC , Ti_3AlC_2 and Cr_2AlC) also present promising corrosion resistance in those heavy liquid metal environments. The coating of those Max-phases on steel substrate could also be possible; however, the electrical conductivity, thermal conductivity and mechanical properties of those Max-phases must also be under consideration.

In summary, the results of our present research confirms that among all test materials, elemental Mo and those 3 kinds of Max-phases (Ti_2AlC , Ti_3AlC_2 and Cr_2AlC) are the most promising candidates to be applied as PCC material in liquid metal batteries. In addition, considering about the price and manufacture of the cell, coating of those promising materials on a suitable substrate might be the most economically reasonable method.

References

- [1] Li HM, Yin H, Wang KL, Cheng SJ, Jiang K and Sadoway DR (2016) Liquid metal electrodes for energy storage batteries. *Adv. Energy Mater.* 2016, 6, 1600483: 1-19. DOI: 10.1002/aenm.201600483
- [2] Kim HJ, Boysen DA, Newhouse JM, et al (2013) Liquid metal batteries: Past, present and future. *Chem. Rev.* 2013, 113, 2075-2099
- [3] Wang K, Jiang K, Sirk AHC, Sadoway DR (2014) Lithium-antimony-lead liquid metal battery for grid-level energy storage. *Nature* 514, 348-350. DOI: 10.1038/nature13700
- [4] Wittingham MS (2012) History, evolution, and future status of energy storage. *Proceedings of the IEEE.* Vol. 100, 1518-1534
- [5] Nardelli PHJ, et al (2014) Models for the modern power grid. *Eur. Phys. J. Special Topics* 223, 2423-2437 (2014). DOI: 10.1140/epjst/e2014-02219-6
- [6] Li HM, Wang KL, Cheng SJ and Jiang K (2016) High performance liquid metal battery with environmentally friendly antimony-tin positive electrode. *ACS Appl. Mater. Interfaces.* 2016, 8, 12830-12835. DOI: 10.1021/acsami.6b02576
- [7] Vikström H, Davidsson S and Höök M (2013) Lithium availability and future production outlooks. *Appl. Energy*, 2013, 110, 252-266
- [8] Gruber PW, Medina PA, Keoleian GA, Kesler SE, Everson MP and Wallington TJ (2011) Global lithium availability: A constraint for electric vehicles? *J. Ind. Ecol.* 2011, Vol. 15, Num. 5, 760-775. DOI: 10.1111/j.1530-9290.2011.00359.x
- [9] Heinzl A, Weisenburger A, Müller G (2017) Corrosion behavior of austenitic steel AISI 316L in liquid tin in the temperature range between 280 and 700°C. *Materials and Corrosion.* 2017; 68:831-837. DOI: 10.1002/maco.201609211